Twenty-First-Century Multimodel Subtropical Precipitation Declines Are Mostly Midlatitude Shifts

JACK SCHEFF AND DARGAN FRIERSON

Department of Atmospheric Sciences, University of Washington, Seattle, Washington

(Manuscript received 13 July 2011, in final form 2 December 2011)

ABSTRACT

Declines in subtropical precipitation are a robust response to modeled twenty-first-century global warming. Two suggested mechanisms are the ''dry-get-drier'' intensification of existing subtropical dry zones due to the thermodynamic increase in vapor transport and the poleward expansion of these same dry zones due to poleward shifts in the modeled general circulation. Here, subtropical drying in the Intergovernmental Panel on Climate Change (IPCC) Fourth Assessment Report multimodel archive is compared to each of these two mechanisms. Each model's particular, biased, and seasonally and zonally varying mean state is considered relative to the location of that model's predicted changes, and these relationships are recorded in a common framework that can be compared across models.

The models have a strong tendency to reduce precipitation along the subtropical flanks of their existing midlatitude cyclonic precipitation belts. This broad result agrees with the poleward expansion mechanism and with a poleward storm-track shift in particular. In contrast, the models have no clear tendency to reduce precipitation in the central nor equatorward portions of their subtropical dry zones, implying that the thermodynamic mechanism is broadly unimportant for the precipitation reductions. This is unlike the response of precipitation minus evaporation, which robustly declines in large portions of these regions, especially over the oceans.

The models also tend to increase precipitation in their wet deep tropical areas, but this is not as robust as the above reduction in the subtropical midlatitudes. High-latitude precipitation increases are the most robust precipitation changes of all in this framework.

1. Introduction

One of the most ubiquitous responses of current global climate models (GCMs) to greenhouse warming is the tendency to reduce climatological precipitation in much of the global subtropics and to increase it throughout the high latitudes (Solomon et al. 2007), potentially on time scales of a few decades or less (Seager et al. 2007). Here we compare two prominent, independent characterizations of the twenty-first-century precipitation responses in the World Climate Research Programme's (WCRP's) Coupled Model Intercomparison Project phase 3 (CMIP3) multimodel dataset (Meehl et al. 2007a) prepared for the Intergovernmental Panel on Climate Change (IPCC) Fourth Assessment Report (AR4) (Solomon et al. 2007), with a focus on the robust large-scale decreases in the subtropics.

Corresponding author address: Jack Scheff, Department of Atmospheric Sciences, University of Washington, Box 351640, Seattle, WA 98195-1640.
E-mail: jscheff@u.washington.edu

DOI: 10.1175/JCLI-D-11-00393.1

a. Fixed-circulation precipitation response from thermodynamics alone (dry-get-drier)

The first of these two mechanisms we call the *thermodynamic* or *dry-get-drier* theory: the idea that under global warming with constant general circulation and constant (low-level) relative humidity, large-scale wet areas would get wetter and dry areas would get drier, simply due to local moist thermodynamic and energetic constraints (e.g., Boer 1993; Trenberth 1998; Betts 1998; Wetherald and Manabe 2002; Allen and Ingram 2002; Held and Soden 2006).

The argument (after Held and Soden 2006) is as follows: under the above scenario, absolute humidity would increase everywhere, following Clausius–Clapeyron scaling, $\sim 7\%\ \mathrm{K}^{-1}$ at earth temperatures. With unchanged circulation, this implies that moisture transport would increase, and thus so would column-integrated moisture convergence, still at roughly $7\%\ \mathrm{K}^{-1}$. Climatologically, this convergence must equal precipitation (P) minus actual evaporation (E) at the surface, using the column water budget. So the pattern of climatological $P - E$

would also amplify at 7% K^{-1}, with negative $P - E$ (''dry'') regions becoming more negative, and positive $P - E$ (''wet'') regions becoming more positive. Furthermore (goes this argument), since E is tied to the local surface energy supply, which is solar-dominated, E cannot change much—so the bulk of this $P - E$ amplification would be accomplished by changes in P. Thus, roughly, P would increase where and when $P - E > 0$; and P would decrease where and when $P - E < 0$ (dry-get-drier).

In particular, we would expect to find robust modeled decreases in P roughly associated with the *subtropical* ocean basins since these are the main regions of large excesses of actual E over P, or atmospheric water export (especially in the annual mean). Furthermore, within these areas, we would expect this mechanism to indiscriminately reduce both the tropical P equatorward of the driest zone, and the midlatitude P poleward of the driest zone, as long as the amount of this P is significantly less than local E.

Held and Soden (2006; their Figs. 7 and 8) provide evidence that the CMIP3 model hydroclimate responses to twenty-first-century global warming roughly follow the expectations from the above framework, at least in the multimodel mean and at planetary scales. This seems especially true for the more basic prediction that the $P - E$ field will amplify.

b. *Precipitation responses due to robust poleward expansion of the circulation*

The second, distinct type of phenomena in the CMIP3 twenty-first-century output that we will consider are the well-known robust poleward shifts of some general circulation features, which also imply drying in the subtropics.

Yin (2005) shows that in the zonal mean, the midlatitude storm-track activity (high-pass eddy kinetic energy) shifts poleward during the twenty-first-century in most models. This behavior is seen in both hemispheres and in summer as well as in winter. Collocated with these storm-track movements are poleward shifts in P. In such a shift, P would increase on the existing seasonal storm track's poleward flank, and decrease on its equatorward flank, which is located in the subtropics—and so we have another mechanism working to reduce P in subtropical latitudes, especially over the oceans, where the storm tracks are most pronounced. However, unlike the equal opportunity dry zone P reduction we would expect from the thermodynamic theory, for a midlatitude shift (in a given season) we would expect a much clearer decline in the mostly midlatitude-forced P poleward of the driest zone, than in the mostly tropical P equatorward of the driest zone. Similar twenty-first-century storm-track shifts have been noted in the CMIP3 ensemble by Lorenz and DeWeaver (2007) and Ulbrich et al. (2008), and in individual GCMs by Fyfe (2003), Fischer-Bruns et al. (2005), and Bengtsson et al. (2006).

In addition, Lu et al. (2007) find that in almost every CMIP3 model and in both hemispheres, the boundary between the Hadley and Ferrel cells (measured as the latitude of the subtropical zero of the Eulerian mean meridional streamfunction at 500 mb) shifts on the order of 1° poleward per hemisphere with strongly forced twenty-first-century global warming, and Frierson et al. (2007) find a similar response in an idealized GCM. Presumably, this is associated with a poleward expansion of the region of zonal-mean descent associated with the driest part of the subtropics, a situation that would again be expected to suppress the subtropical flank of midlatitude-driven P. Indeed, the latitude where zonal mean $P - E$ switches from its subtropical negative values to its midlatitude positive values also shifts poleward in Lu et al. (2007), and the distance it shifts in a given model is highly correlated with the distance moved by the Hadley–Ferrel boundary in that model. So, this phenomenon should also explain some of the robust subtropical P reductions. Notably, it would also only affect parts of the subtropics poleward of the driest zone in a given season since the descent expands poleward at the expense of midlatitude ascent, but it does not also expand equatorward at the expense of tropical ascent.

Unlike the thermodynamic amplification of $P - E$, these poleward shifts do not stem from any known fundamental principle; they are simply a common feature of essentially all current global warming simulations, with several competing postfacto explanations in the literature (e.g., Lorenz and DeWeaver 2007; Chen et al. 2008; Lu et al. 2010; Riviere 2011; Butler et al. 2011; Kidston et al. 2011; Ma et al. 2012). It is not even clear whether the shifts of the storm tracks and of the meridional circulation occur for the same reason, as discussed by Previdi and Liepert (2007). The relationships between these centennial-scale model responses and various much stronger but shorter-term poleward-migrating trends in the *observed* and/or reanalyzed subtropical to midlatitude circulation are also unclear. These recently shifting features include the upper-tropospheric baroclinic jets (Fu et al. 2006; Archer and Caldeira 2008; Fu and Lin 2011) and tropopause break (Seidel and Randel 2007), as well as the storm tracks (McCabe et al. 2000; Fyfe 2003) and associated annular mode indices (Marshall 2003; Thompson et al. 2000), and the mean meridional circulation (Hu and Fu 2007). However, the only aspect needed for this study is that poleward shifts of both the meridional circulation and of the storm track should dry the model subtropics poleward, but not equatorward, of the driest zones, unlike the dry-get-drier thermodynamic response.

TABLE 1. The 19 WCRP CMIP3 (Meehl et al. 2007a) climate models (used for the IPCC AR4) with monthly output from scenarios 20C3M and A2 analyzed in this study.

Model name and origin	Abbreviation	Notes
Bjerknes Center for Climate Research (BCCR) Bergen Climate Model, version 2.0 (BCM2.0), Norway	BCCR	
Community Climate System Model, version 3 (CCSM3), United States	CCSM3.0	
Canadian Centre for Climate Modelling and Analysis (CCCma) Coupled General Circulation Model, version 3.1 (CGCM3.1) (T47), Canada	CCCma	
Centre National de Recherches Météorologiques Coupled Global Climate Model, version 3 (CNRM-CM3), France	CNRM	
Commonwealth Scientific and Industrial Research Organisation Mark version 3.0 (CSIRO Mk3.0), Australia	CSIRO3.0	
CSIRO Mk3.5, Australia	CSIRO3.5	
ECHAM5/Max Planck Institute Ocean Model (MPI-OM), Germany	MPI	Removed erroneous extra years 2001–2100 from 20C3M before concatenating with A2.
ECHAM and the global Hamburg Ocean Primitive Equation (ECHO-G), Germany/Korea	MIUB	
Geophysical Fluid Dynamics Laboratory Climate Model version 2.0 (GFDL CM2.0), United States	GFDL2.0	
GFDL CM2.1, United States	GFDL2.1	This model did not archive surface latent heat fluxes or evaporation, and therefore was **omitted** in the analyses requiring evaporation output.
Goddard Institute for Space Studies Model E-R (GISS-ER), United States	GISS	
Istituto Nazionale di Geofisica e Vulcanologia SINTEX-G (INGV-SXG), Italy	INGV	
Institute of Numerical Mathematics Coupled Model, version 3.0 (INM-CM3.0), Russia	INM	
L'Institut Pierre-Simon Laplace Coupled Model, version 4 (IPSL CM4), France	IPSL	20C3M and A2 both contain year 2000 output; used 20C3M version of this year only.
Model for Interdisciplinary Research on Climate 3.2, medium-resolution version [MIROC3.2(medres)], Japan	MIROC	
Meteorological Research Institute Coupled General Circulation Model, version 2.3.2 (MRI-CGCM2.3.2), Japan	MRI	
Parallel Climate Model (PCM), United States	PCM	
Met Office (UKMO) Hadley Centre Climate Model, version 3 (HadCM3), United Kingdom	HadCM3	
UKMO Hadley Centre Global Environmental Model, version 1 (HadGEM1), United Kingdom	HADGEM1	

2. Model output analyzed

This study assesses these two mechanisms in monthly-mean output for years 1980–2099 from the CMIP3-archived climate model runs of scenarios Twentieth Century Climate in Coupled Models (20C3M) and "A2." Scenario 20C3M uses historical climate forcings, so we start the analysis in 1980 so as to avoid the period of strong aerosol forcing in the middle of the twentieth century and isolate the response to greenhouse warming. Scenario A2 smoothly takes the end of 20C3M around the year 2000 as its initial condition, and then greatly increases the level of CO_2 by 2099. This scenario is chosen for its presumably high signal-to-noise ratio for effects of greenhouse warming, with the downside that CMIP3 does not include it for a few models.

However, 19 usable models still remain, and are listed in Table 1 along with any exceptions to the above procedure. They will be used in the analyses based on the P climatology. For the analyses involving the $P - E$ climatology, we are forced to drop one of these models because its surface latent heat fluxes, from which E has to be calculated, are not available, so this part is done using only 18 models (see Table 1). For simplicity, the heat of vaporization (for converting from latent heat flux to E) is taken to be a constant, 2.45×10^6 J kg^{-1}. (We do

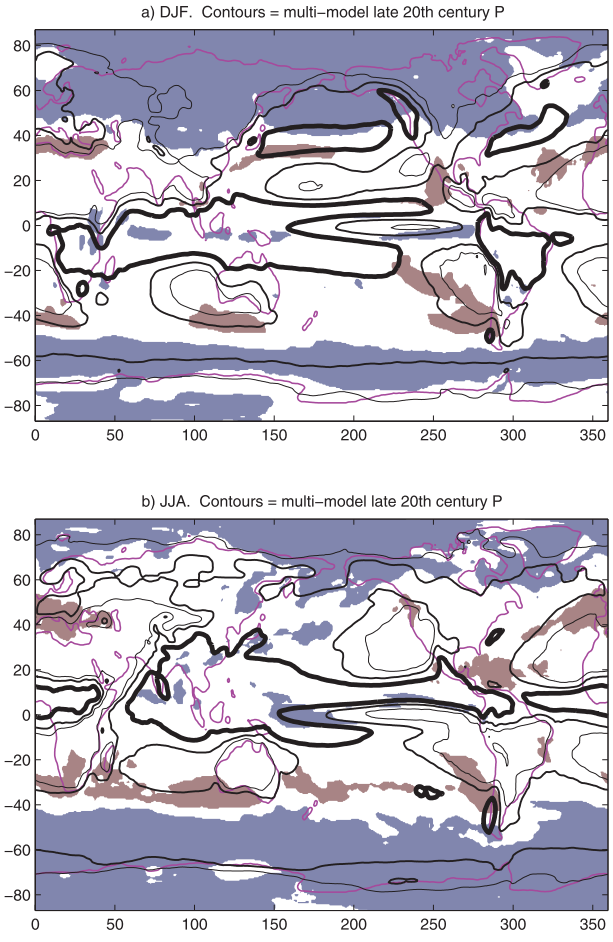

FIG. 1. Black contours are the late twentieth-century multimodel climatological P (1, 2, and 5 mm day^{-1} lightest to boldest), and colors are the locations of robust multimodel twenty-first-century P decreases (red) and increases (blue): (a) December–February only and (b) June–August only.

not attempt to use the heat of sublimation since we are mainly concerned with subtropical locations.) If for a given model and scenario there is more than one run archived, we take only the run numbered "1."

For each model and for all 12 overlapping 3-month seasonal means of the year (December–February, January–March, . . . , November–January), for P and for $P - E$, we compute the following fields in latitude and longitude: the 1980–99 and 2080–2099 climatologies, the full $N = 120$ linear trend (1980–2099), and whether or not this trend is significant at 95% (using a two-tailed t test). However, we are not making any formal, probability-based claim about the statistical significance of our overall result in this study. This would require a more realistic null hypothesis than no change in local climate under global warming and would also require consideration of multiplicity and field significance (e.g., Wilks 2006; Livezey and Chen 1983). Rather, at each location and in each season, we are simply using this linear significance as a qualitative indicator of the presence or absence of a visually clear trend, which will then be collated into a broader picture of the time behavior of the entire field in section 4 below.

Our t test explicitly accounts for the lag-one autocorrelation r_1 of the residuals, by multiplying the variance of the trend estimator by $(1 + r_1)/(1 - r_1)$ (e.g., Wilks 2006; Santer et al. 2000). For most locations (multimodel average of 95% of all season grid points, lowest model: >91%), $|r_1| < 0.2$, with no particular sign preference. However, some models have sizable areas in the tropical Pacific where r_1 is of order -0.4 (not shown), which would lead to visually apparent trends being found insignificant, if not corrected for. These negative tropical Pacific autocorrelations might be due to the ~2-yr periodicity of El Niño/La Niña in many climate models (e.g., Lin 2007). Regardless, there do not seem to be large regions with $r_1 > +0.2$ in the models examined (multimodel average of 2.4% of all season grid points, highest model: 5.3%). This suggests that a linear trend is indeed a good statistical model for these time series, and cursory visual inspection (not shown) seems to back this up.

3. Traditional multimodel ensemble analysis

We first examine the CMIP3 ensemble as a multimodel whole, along the lines of the studies cited in section 1 above. For two representative seasons (December–February and June–August), we plot the regions of robust multimodel twenty-first-century P change against the multimodel mean late twentieth-century seasonal climatologies of P (Fig. 1) and of $P - E$ (Fig. 2).

To define "robust" multimodel change, we require the magnitude of the multimodel mean of the twenty-first-century change to exceed the intermodel standard deviation of this change. In each model, we use the raw difference between the computed late twenty-first-century and late twentieth-century climatologies to measure this change. These choices are all made to be consistent with the graphics in the IPCC Fourth Assessment Report (Meehl et al. 2007b; their Fig. 10.9, middle column), which also analyzes CMIP3 output. The multimodel means and standard deviations of any desired quantity (e.g., twenty-first-century change) are computed by bilinear interpolation of each individual model's field of that quantity onto a common $0.5° \times 0.5°$ fine grid.

Our robust P reduction regions are almost identical to those stippled in the above-mentioned IPCC figure, despite their use of the somewhat weaker A1B scenario, and despite our resulting use of fewer models. [The only exception is our area of robust reduction in and near the

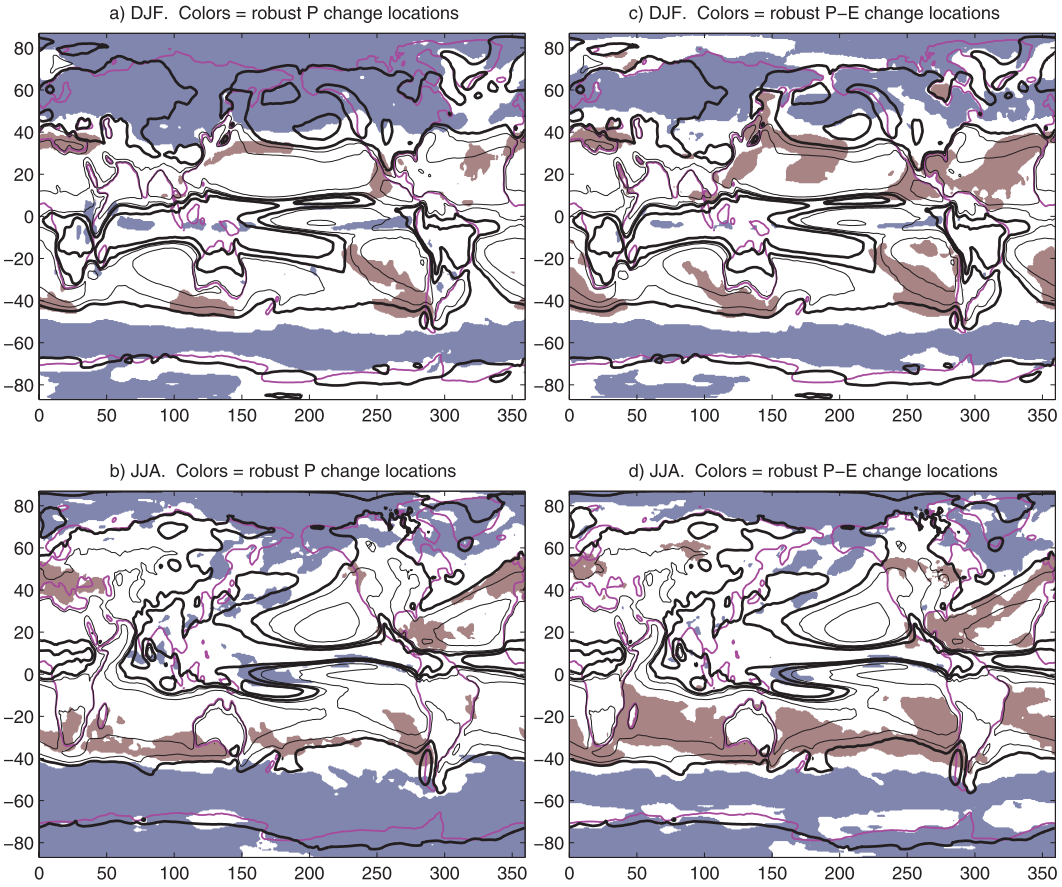

FIG. 2. (a),(b) As in Fig. 1, but black contours are now late twentieth-century multimodel climatological $P - E$ (-2.5, -0.5 mm day^{-1} light; $+0.5$, $+2.5$ mm day^{-1} bold; 0 contour not shown). Colors (reproduced from Fig. 1) are the locations of robust multimodel twenty-first-century P decreases (red) and increases (blue). (c),(d) As in (a),(b), but colors are now locations of robust $P - E$ decreases (red) and increases (blue).

Caribbean Sea in June–August, which is not stippled in the Meehl et al. figure.]

In both December–February (Fig. 1a) and June–August (Fig. 1b), the robust declines in P (red regions) are rarely found near or equatorward of the initial subtropical P minima. Rather, they are mostly found well poleward of the minima, along the subtropical flanks of the model midlatitude wet zones in P. Also, these robust P decreases have this same distribution relative to model climatology whether the actual latitude is ''subtropical'' (e.g., the southern Mediterranean and adjacent Atlantic in winter) or ''midlatitude'' (e.g., central Europe and the adjacent Atlantic in summer). This suggests that the poleward expansion of the subtropical dry zones due to circulation change is a dominant factor here. In particular, the frequent symmetric placement of the robust *P increases* immediately poleward of these decreases, following the subpolar flanks of the same midlatitude high-P zones, suggests a *storm-track* shift (e.g., in the Southern Ocean and central North Atlantic in both Figs. 1a and 1b, and in the western North Pacific in Fig. 1a). Also, the declines are located in longitudes with active storm-track–subtropical-high dynamics, further supporting this dynamic interpretation.

The story told by Figs. 2a and 2b, which plot these same robust P changes against the multimodel climatology of $P - E$ (rather than P), is somewhat more complicated. Though the regions of robust P decline do leak into parts of the climatological ''wet'' $P - E > 0$ zones, they have a clear preference for the ''dry'' $P - E < 0$ zones. However, within the $P - E < 0$ zones, the robust P declines are largely restricted to their poleward rims, and they rarely occur in, near, or equatorward of the broad $P - E$ minima as one would expect from thermodynamic drying. Instead, the distribution suggests a dominant role for poleward expansion, and only a secondary, constraining role for the thermodynamic (dry-get-drier) effect.

Major exceptions to this pattern include the regions on the Pacific side of Mexico in winter (Fig. 1a) and in

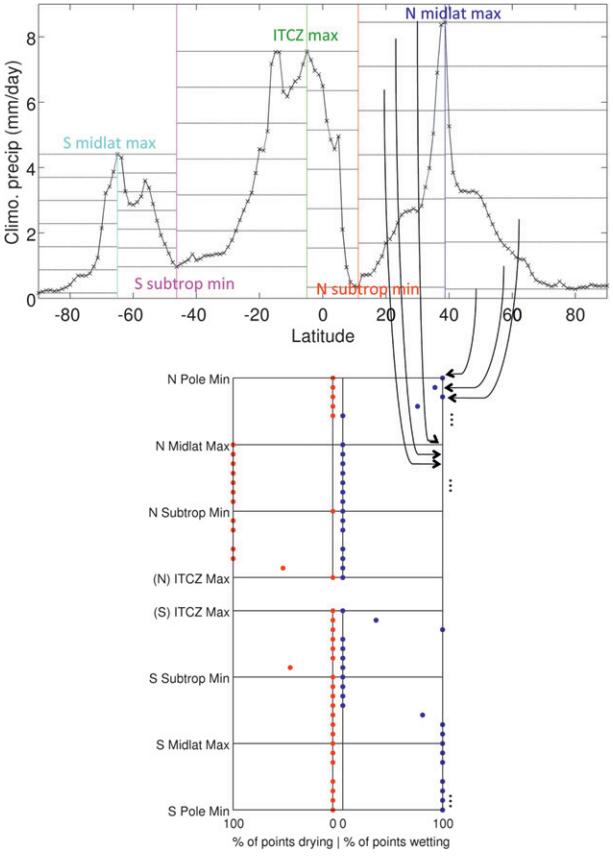

FIG. 3. (top) Black curve shows a sample late twentieth-century climatological P vs latitude profile, from the zonal average of the (290°, 300°E] strip in HadGEM1, March–May. Colored vertical lines show the large-scale features of this profile as defined by the criteria in the appendix (the peak near 15°S is slightly lower than the ITCZ, and thus is not prominent enough to be a feature). Black horizontal lines show the boundaries of the interfeature P bins to which each point of the profile is assigned for response-recording purposes, according to section 4a. (bottom) The percentage d of latitudes with significant twenty-first-century (1980–2099) drying trends in P, and the percentage w of latitudes with significant twenty-first-century wetting trends in P, for each bin of each segment of this profile. The bins are arranged in quasi-geographic order within each segment, illustrated by the black arrows: from lowest P to highest P going down the top segment, from highest P to lowest P going down the next segment, and so forth. Ordinates with missing data correspond to bins that do not contain any points.

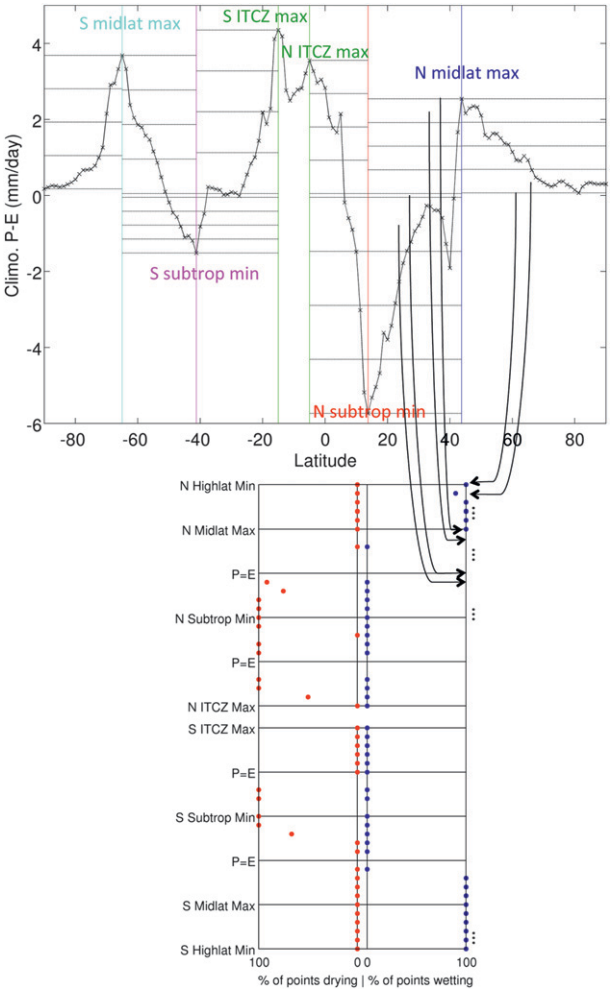

FIG. 4. (top),(bottom) As in Fig. 3, but using the $P - E$ profile. Note that two ITCZ peaks are now defined (see appendix). The horizontal axis at (bottom) still records the frequency of significant P trends in each bin, but the bins and features (along the vertical axis) are now defined using climatological $P - E$, as shown at (top) and explained in section 4a.

the Caribbean in summer (Fig. 1b). These regions feature robust multimodel drying, and they are both located where the base of the model North Atlantic seasonal storm track in P meets the model ITCZ. In turn, Figs. 2a and 2b show that these drying areas strongly coincide with the $P - E$ minimum, in latitude if not in longitude. So this is the one region where the above description seems to break down, though it could be argued that a poleward movement of storms might still negatively affect this area since it is the most equatorward part of the apparent midlatitude-driven P feature. Regardless, though, this is at least some evidence that idealized-looking thermodynamic-type deep subtropical P reductions can occur in the multimodel consensus. [Interestingly, this uniqueness of the Caribbean summer drying response was also noted by Neelin et al. (2006), who considered it a tropical phenomenon.]

These results do not contradict the pure thermodynamic result that $P - E$ patterns amplify with global warming. Figures 2c and 2d plot the regions of robust multimodel seasonal $P - E$ increases and decreases, defined exactly the same way, against the multimodel $P - E$ climatologies from Figs. 2a and 2b. In this view, the regions of robust drying extend much farther

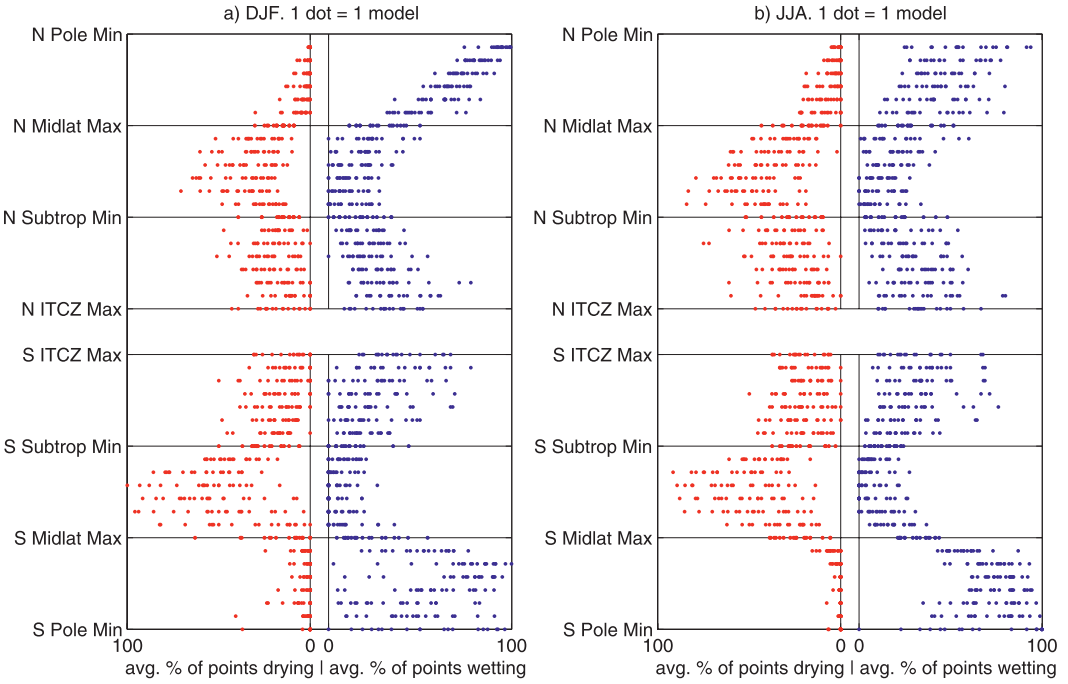

FIG. 5. For each bin of each segment of the (a) December–February and (b) June–August late twentieth-century P climatology profiles, and for each single GCM, the percentages d and w of latitudes classified in that bin for which seasonal P significantly declines and increases over the twenty-first-century (1980–2099) (as in Fig. 3), averaged over all longitude strips globewide for which the P climatology features are defined. At each ordinate, one red (blue) dot represents this average d (w) for one single GCM (1 dot = 1 model).

equatorward, and indeed suggest dry-get-drier plus a poleward shift, as suggested by the detailed water budget study of Seager et al. (2010). It seems that the bulk of robust changes in $P - E$ need not be accomplished by robust changes in P, contrary to the argument in Held and Soden (2006). [The meridional gradient in E and in Held and Soden's scaling for the small response of E to warming cannot account for this discrepancy—see the derivation from their scaling in Scheff (2011).]

The results for the remaining seasons (not shown) closely resemble those presented above for December–February and June–August.

4. Model-by-model analysis

A geographic multimodel robustness measure like that used above may miss some behavior that is robust in a feature-relative sense since the climatological feature in question (e.g., subtropical dry zone or midlatitude wet zone) is located at different (biased) latitudes and/or longitudes in different models. Conversely, one might also be interested in the extent of the intermodel diversity of feature-relative P behavior, in addition to the robust similarities. Therefore, we also examine each one of the GCMs in Table 1 *individually*, based on aspects of each model's climatology. We refer to this as the *model-by-model* approach.

To conduct such an analysis, we need some common criteria to define the large-scale ITCZ maximum or maxima, subtropical minima, and midlatitude maxima of seasonal P and $P - E$ in each model, so as to classify the locations of the respective P responses relative to them. It would be relatively simple to do this in the planet-wide zonal mean. However, these features, and the change patterns associated with them, are often far from zonal (as can be seen in Figs. 1 and 2) and so with zonal averaging there is a danger of assigning some part of a change region to the wrong climatological feature, and/or smearing conceptually similar changes across tens of degrees of latitude. So, we separately define these features along many different longitudes, using the procedures given in the appendix. We use zonal means over 36 pole-to-pole meridional strips (0, 10]°E, (10, 20]°E, . . . , (350, 360]°E, rather than the individual grid meridians, so as to smooth out some of the noise while preserving the ability of this technique to resolve the above slanting of the features. A relatively simple example of such a local profile or transect of single-model seasonal P, with its features defined as in the appendix, is shown at the top of Fig. 3; and the corresponding profile of $P - E$ with its own

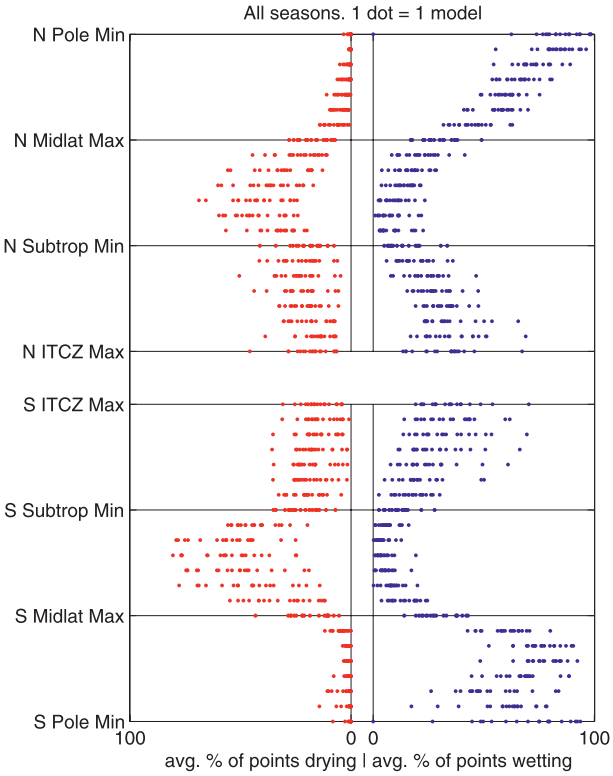

FIG. 6. The mean of all 12 plots in the family of Figs. 5a and 5b. For each bin of each segment of the late twentieth-century seasonal P climatology profile, and for each single GCM, the percentages d and w of latitudes classified in that bin for which seasonal P significantly declines and increases over the twenty-first century (1980–2099) (as in Fig. 3), averaged over all longitude strips globewide for which the P climatology features are defined, and then over all 12 overlapping 3-month seasons. At each ordinate, one red (blue) dot represents this average d (w) for one single GCM (1 dot = 1 model).

features defined as in the appendix is shown at the top of Fig. 4.

a. Classifying, recording, and concatenating the single-model relative behaviors

We can now record the meridional locations of the significant twenty-first-century *changes* in strip-mean model P relative to these features, in a way that can be combined across many models, longitudes, and/or seasons into a single dataset. We first explain this process for the analysis relative to initial climatological P, as opposed to $P - E$.

First, we discard the small minority of model–season–transect-hemispheres for which the midlatitude maximum and subtropical minimum in P climate were not defined (see appendix). We then conceptually split the remaining profiles at the latitudes of their features (omitting the intra-ITCZ latitudes if multiple ITCZs were defined). Thus, each half-transect is decomposed into three roughly monotonic segments: the geographically appropriate flank of the (relevant) ITCZ, the subtropical flank of the storm track, and the subpolar–polar flank of the storm track. This can be pictured in both hemispheres with the aid of the example profile in Fig. 3.

On each of these profile-segments, we now note the overall minimum and maximum P values. Normally, these are the values at the segment end latitudes (i.e., the defined large-scale features) by design; the only exception being the minimum P value of the polar flank of the storm track, which might not quite be attained at the pole itself (e.g., the top of Fig. 3 just south of 80°N). We then divide each segment into six equal bins *according to P value (not latitude)*, and classify each point of the initial profile according to the P bin it belongs to (e.g., which rectangle in the top of Fig. 3 it lies in): 0 to 1/6 of the way up, 1/6 to 2/6 of the way up, . . . , or 5/6 to 6/6 of the way up from the segment's P minimum to its P maximum. The minimum and maximum points themselves are put into bins of their own at the top and bottom, for eight P bins total per segment.

Then, for each individual P bin (of each feature-to-feature segment of our particular profile), we define the "fraction of points drying" d to be the proportion of that bin's points (grid latitudes) for which the model's twenty-first-century trend of the 10°-zonal-mean seasonal P is significant at 95% (see section 2) and negative. Similarly, the "fraction of points wetting" w is defined to be the proportion of the bin's grid latitudes for which this same trend is significant at 95% and positive. If in fact no grid latitudes fall into this P bin for this particular profile (e.g., the bin 2/6 to 3/6 of the way up from the north subtropical minimum to the ITCZ in the example of Fig. 3), then d and w are left with a missing-value placeholder. The bottom of Fig. 3 shows d and w plotted (in percent form) for each bin and segment of the example initial transect shown above it.

Note that because the feature-to-feature $P(y)$ profile segments are not actually monotonic, a single P bin may not contain latitudes that are all adjacent to each other—and so the ordinates within each rectangle of a plot like the bottom of Fig. 3 cannot be interpreted in a purely geographic sense. This can be seen in the top bin of the south-subtropical-minimum-to-ITCZ segment in the example profile. However, this approach has the advantage of low sensitivity to the exact latitudes of the features and high sensitivity to the precipitation (or $P - E$) structure, which is the immediately relevant variable to the theories discussed in section 1. To see this, consider the classification of the points around 30°S (just equatorward of the broad subtropical minimum) in Fig. 3 (top). The above system places them conceptually "close" to the

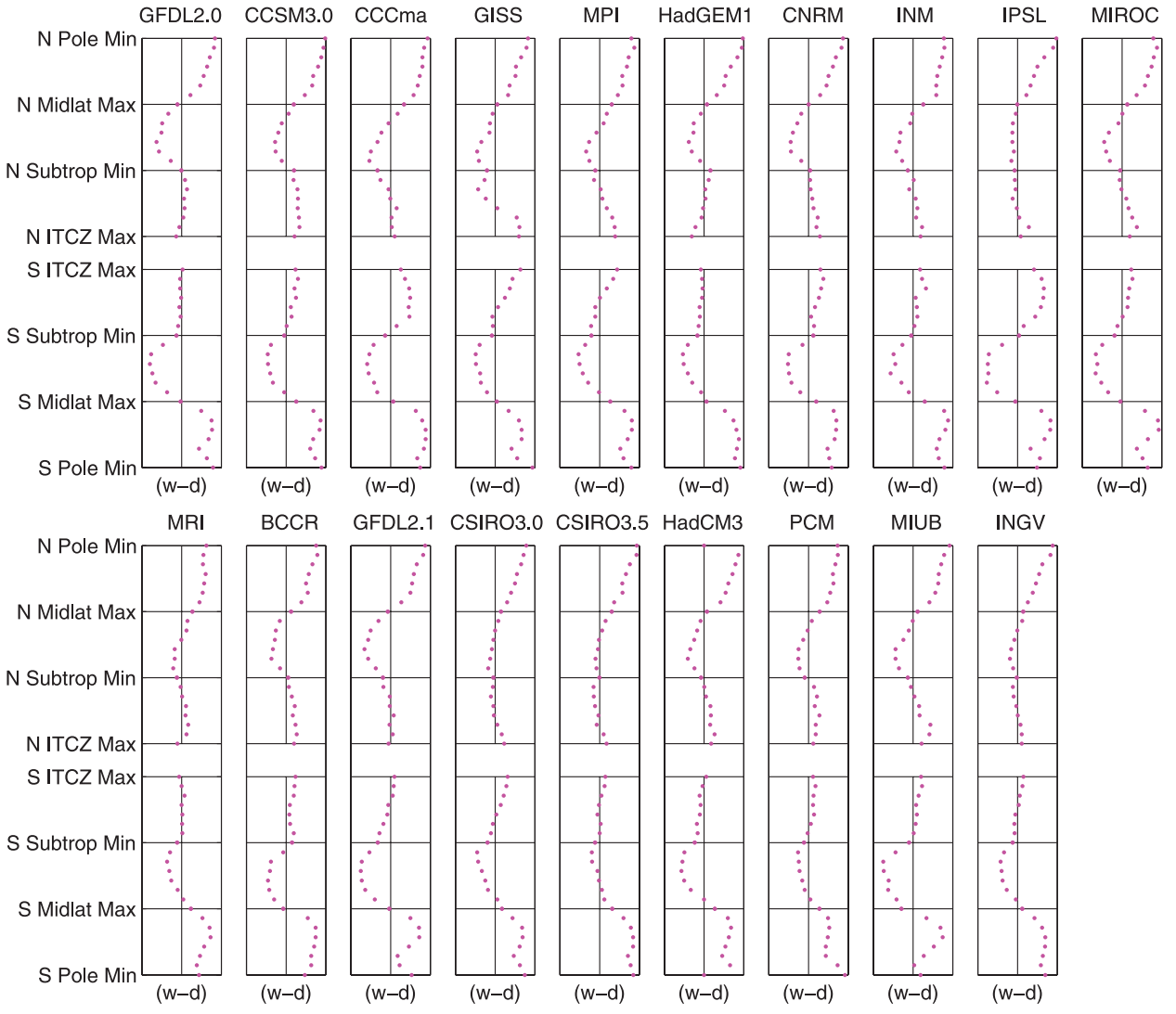

FIG. 7. As in Fig. 6, but each GCM is now plotted on a separate pair of axes, and the difference $w - d$ is plotted for conciseness. Each horizontal axis runs from −1 (all drying; none wetting) on the left to 1 (all wetting; none drying) on the right. For full model names, see Table 1.

subtropical minimum, as thinking about the ideas in section 1 demands, rather than nearly halfway to the ITCZ, as a latitude-based classification would imply. This is the main motivation for using P, as opposed to latitude, to define the bins within each segment.

Also, the individual bins of each strip are usually smaller than the large-scale regions of P change (or nonchange) and will often be enveloped entirely by one of them. Thus, by far the most common values of the pair (d, w) for a bin will be (0, 0), (1, 0), or (0, 1), as can be seen in Fig. 3. So, if we average together the equivalents of the bottom of Fig. 3 for many profiles (as we will do in section 4b shortly), we can think of the average d at each bin "coordinate" as the *fraction of profiles for which that feature-relative "location" dries in P*, and similarly for the average w, since the average of a list of zeroes and ones is the fraction of its entries that are ones.

The procedure for recording the locations of the significant P changes in each strip relative to the $P - E$ climatology features, as opposed to the P climatology features, is identical except for one key difference, illustrated in Fig. 4. Namely, if any of the individual feature-to-feature $P - E$ profile segments takes on both positive ($>+0.05$ mm day^{-1}) and negative (<-0.05 mm day^{-1}) values of $P - E$, we declare both $+0.05$ mm day^{-1} and -0.05 mm day^{-1} to be $P - E$ bin boundaries, and name the resulting bin the "$P = E$" bin. We then bound the segment's remaining $P - E$ bins at 1/4, 2/4, and 3/4 of the way from $+0.05$ mm day^{-1} up to the $P - E$ maximum, and at 1/4, 2/4, and 3/4 of the way

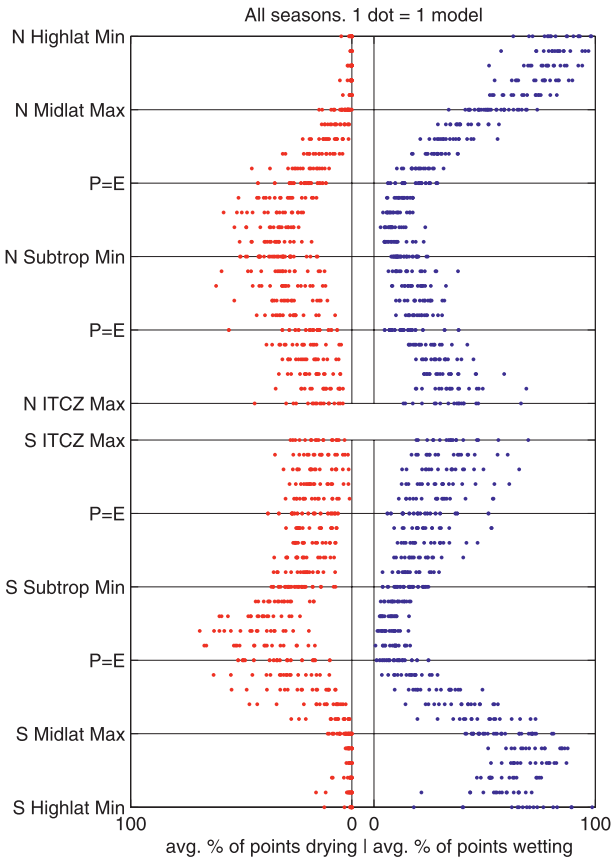

FIG. 8. As in Fig. 6, but the vertical axis is now the $P - E$ profile, not the P profile. For each bin of each segment of the late twentieth-century seasonal $P - E$ climatology profile, and for each single GCM, the percentages d and w of latitudes classified in that bin for which seasonal P significantly declines and increases over the twenty-first century (1980–2099) (as in Fig. 4), averaged over all longitude strips globewide for which the $P - E$ climatology features are defined and have the default sign configuration (end of section 4a), and then over all 12 overlapping three-month seasons. At each ordinate, one red (blue) dot represents this average d (w) for one single GCM (1 dot = 1 model).

from the $P - E$ minimum up to -0.05 mm day^{-1}, for nine interior bins total of varying width. For segments that retain the same sign throughout, we simply use 1/4, 2/4, and 3/4 of the way from the $P - E$ minimum up to the $P - E$ maximum, for four equal interior bins.[1] This is all done because the *sign* of climatological $P - E$ is needed to evaluate the relevance of the dry-get-drier/thermodynamic theory discussed in section 1a, and because $P - E \sim 0$ has its own physical interpretation when the underlying surface is land (see the caution at the end of the appendix). This is another key reason why we bin each segment according to hydroclimate value (instead of latitude) for classification purposes.

Ordinarily, the subtropical minimum of each $P - E$ half-profile is negative, and the other defined features (as well as all points poleward of the midlatitude maximum) are positive, so that the subtropical flank of the midlatitude maximum and the ITCZ flank are split at $P - E \sim 0$ in this way, while the polar flank of the midlatitude maximum is not (as in the example in Fig. 4). We call this the default configuration. Segments of some profiles will behave differently on occasion, and thus will be binned differently and must be plotted separately. These segments are examined in Scheff (2011); the ($P - E$)-relative analyses in the present article will only include each transect's *default*-configured segments (>90% of the ITCZ flanks and equatorward midlatitude flanks, and >62% of the poleward midlatitude flanks). However, the P-relative analyses (e.g., immediately below) will still include *all* segments.

b. *Displaying the family of single-model feature-relative P responses to global warming*

Figure 5 shows every GCM's d (fraction of points in bin drying) and w (fraction of points in bin wetting) profiles with respect to the meridional P features and P bins (as in Fig. 3), averaged bin-wise over all longitude strips for which the features in question were defined, for December–February (Fig. 5a) and June–August (Fig. 5b), one dot per model. As discussed above, these values can be roughly thought of as the *fraction of longitudes that get significantly drier or wetter (in P)* in response to global warming, for a particular feature-relative meridional location, model, and season. Figure 6 shows the bin-wise mean of all 12 three-month average plots of this type [December–February (Fig. 5a), January–March, . . . , November–January].

One striking aspect of Figs. 5 and 6 is the extreme rarity of significant drying at high latitudes poleward of the midlatitude maxima, especially in the climatologically driest (most poleward-plotted) bins. In contrast, the wetting response is very common in these locations, excessively so in the winter hemispheres (top of Fig. 5a and bottom of Fig. 5b), where *all* models feature clear high-latitude precipitation increases. This is consistent with the large areas of robust wetting at high latitudes in the multimodel ensemble plots (Fig. 1), and could potentially be a consequence of both thermodynamic wetting and of poleward storm-track shifts.

Moving further equatorward in Figs. 5 and 6, we can see that widespread drying is clearly more common than

[1] On the rare occasion that one of the segment's global extrema is actually in the interval (-0.05 mm day^{-1}, $+0.05$ mm day^{-1}), then we still treat this interval separately, so there will be five interior bins.

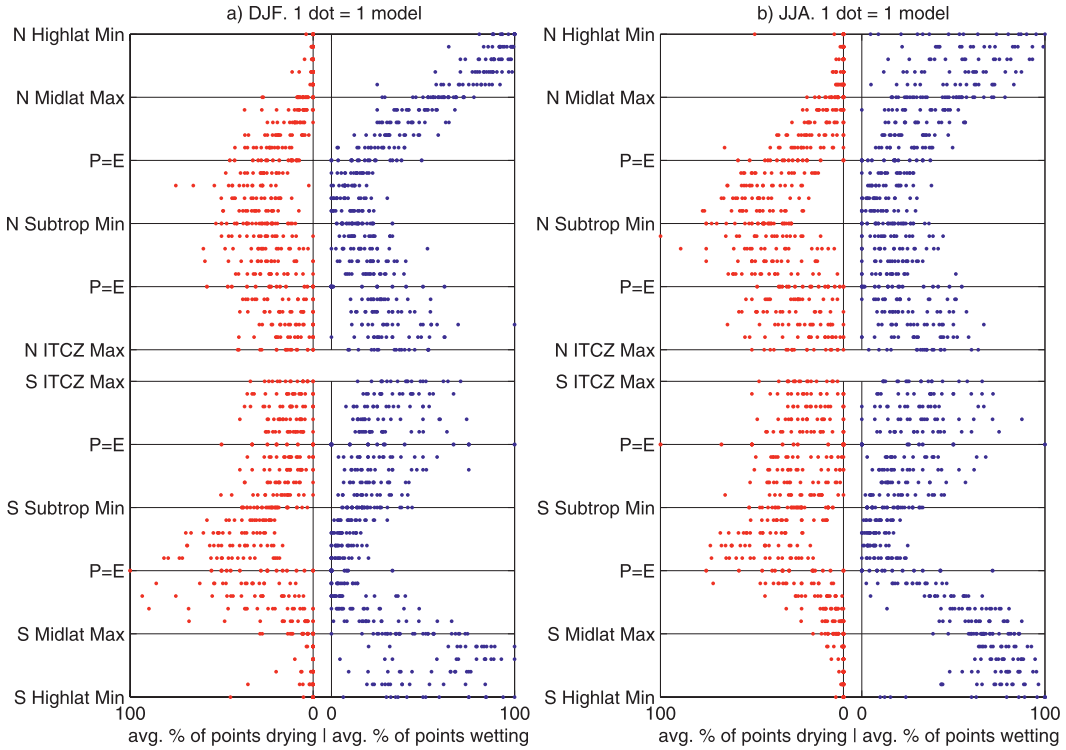

FIG. 9. As in Fig. 8, but for (a) December–February and (b) June–August only. For each bin of each segment of the December–February and June–August late twentieth-century $P - E$ climatology profiles, and for each single GCM, the percentages d and w of latitudes classified in that bin for which seasonal P significantly declines and increases over the twenty-first century (1980–2099) (as in Fig. 4), averaged over all longitude strips globewide for which the $P - E$ climatology features are defined and have the default sign configuration (end of section 4a). At each ordinate, one red (blue) dot represents this average d (w) for one single GCM (1 dot = 1 model).

widespread wetting between the subtropical minima and the midlatitude maxima (i.e., on the subtropical flanks of the midlatitude P belts), dramatically so in the Southern Hemisphere. In contrast, at the subtropical P minima themselves, and in the first (driest) few P bins on their equatorward sides, the typical extents of drying and wetting are comparable. That is, all models do decrease deep-subtropical P in some longitudes, but they also all increase deep-subtropical P in about the same number of other longitudes, so there is no clear preference toward drying.

This strongly suggests a key role for the circulation change–driven poleward expansion of the subtropical dry zones (section 1b), rather than their thermodynamically driven, energetically constrained in-place intensification (section 1a), in the above twenty-first-century model P reductions. The pattern also closely parallels the result of the ensemble analysis of section 3 (Fig. 1): no clear P reductions in or equatorward of the subtropical P minima, in contrast to clear P reductions poleward of the minima, which led us to the same conclusion.

It is also notable that significant wetting is somewhat more common than drying near the ITCZ(s) in Figs. 5 and 6, as one might expect from the wet-get-wetter consequence of the thermodynamic theory. However, this response is noticeably weaker than the dominance of apparent dynamic drying between the subtropical minima and midlatitude maxima noted above. This is consistent with the relatively small and fragmented area of robust low-latitude wetting in the ensemble analyses (Fig. 1), compared to the area of robust subtropical–midlatitude drying. One possible explanation may be that different models dry and wet different parts of the deep tropics in response to global warming, as pointed out by, for example, Neelin et al. (2006), and that our method tallies such regional changes, rather than examining the change in the zonal mean.

Figure 7 presents an alternate view of the data in Fig. 6, in which each model's averaged statistics are plotted in separate panels. The difference $w - d$, ranging from -1 to 1, is used in place of w and d themselves for conciseness. The tendency for $w - d$ to cleanly change sign right at the midlatitude P maximum is very widespread, especially in the Southern Hemisphere, again strongly suggesting a storm-track shift as a specific reason

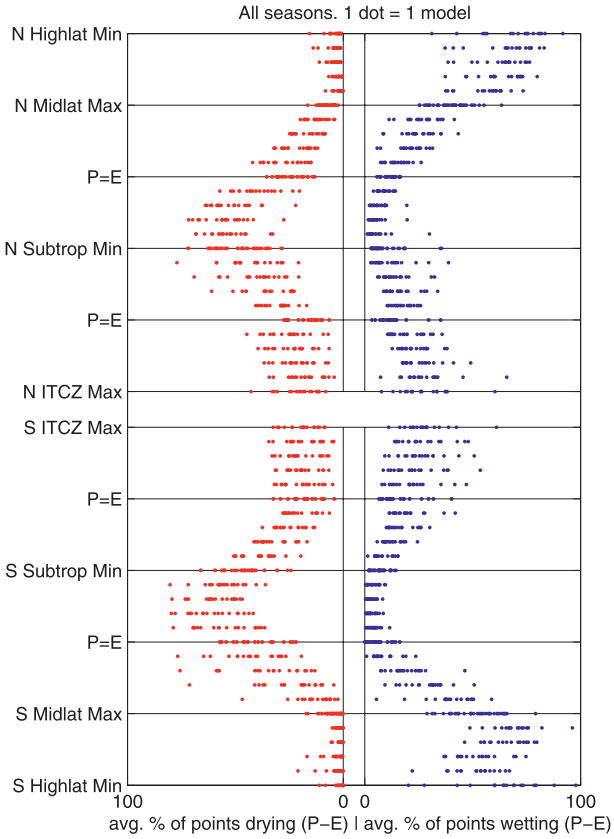

FIG. 10. As in Fig. 8, but for $P - E$ changes. For each bin of each segment of the late twentieth-century seasonal $P - E$ climatology profile, and for each single GCM, the percentages d^* and w^* of latitudes classified in that bin for which seasonal $P - E$ significantly declines and increases over the twenty-first century (1980–2099), averaged over all longitude strips globewide for which the $P - E$ climatology features are defined and have the default sign configuration (end of section 4a), and then over all 12 overlapping 3-month seasons. At each ordinate, one red (blue) dot represents this average d^* (w^*) for one single GCM (1 dot = 1 model).

for the poleward expansion [as opposed to (just) a shift in the Hadley–Ferrel border]. This is also suggested by a fairly common double-peaked structure in the southern high-latitude wetting, with the near-storm-track wetting expected from a shift somewhat separated from the wetting of cold, low-P regions closer to the pole. The aforementioned weakness of both drying near the subtropical minima and wetting near the ITCZ(s), compared to this strong drying between the midlatitude maxima and subtropical minima, is also apparent.

Figure 8 plots the same type of all-appropriate longitude, all-12 season averages of d and w for each GCM as in Fig. 6, except that now d and w have been computed for (and averaged and combined along) the $P - E$ bins and features (as in Fig. 4), instead of the P bins and features. The ubiquity of wetting poleward of the storm-track maxima is still apparent, but the subtropical responses are somewhat weaker in this framework. In the Northern Hemisphere subtropics, the P reductions dominate the increases in only one range of $P - E$ bins (ordinates): poleward of the (negative) subtropical $P - E$ minimum, but not so far toward the midlatitude maximum that $P - E$ has gone positive. This, too, is closely analogous to the corresponding robust ensemble response described in section 3 and again suggests that the thermodynamic mechanism is probably not the main reason for the ''victory'' of the P reductions (otherwise they would dominate equatorward of the $P - E$ minimum as well, nearly to the other zero line) but may play a key constraining role on the poleward side.

The Southern Hemisphere in Fig. 8 is similar, except that the midlatitude $P = E$ bin does not seem to constrain the region of robust P reduction the way it does in the Northern Hemisphere, and the dominance of drying poleward of the subtropical $P - E$ minimum is even more pronounced than in the Northern Hemisphere. In other words, this looks like more of a pure poleward-expansion response. This is a bit unlike the pattern in the traditional ensemble in section 3, where there seems to be more of a preference for the P reductions to lie equatorward (north) of $P = E$.

Figure 9 shows equivalents of Figs. 5a and 5b (individual seasons) for these $P - E$ feature-relative P responses. These are broadly similar to the all-season Fig. 8 above but with some apparent differences. Namely, in the Northern Hemisphere in summer (Fig. 9b, top) deeper-subtropical P reductions are actually somewhat more common than increases; and in the Southern Hemisphere in winter (Fig. 9b, bottom), the region of dominant P declines is more constrained by the midlatitude $P = E$ line than it is in Fig. 8. (The scatter is also increased here since less averaging has been performed.)

Figure 10 is identical to Fig. 8 except that we have now tallied the proportions d^* and w^* of points where $P - E$ significantly declines and increases, defined in the same manner as d and w were for P in section 4a. Note the extent of the robust $P - E$ drying ''victory'' over wetting from just poleward of the tropical $P = E$ bin to just poleward of the midlatitude $P = E$ bin, as might be expected from dry-get-drier modulated by a general poleward shift; consistent with the descriptions in Seager et al. (2010). This confirms the result from the ensemble analysis in section 3 that an overall tendency to reduce $P - E$ in and equatorward of the subtropical minima (Fig. 10) does not have to lead an overall tendency to reduce P there (Fig. 8), despite the clear similarities in the large-scale structure of the diagnostics. We can also see that even in this framework, widespread $P - E$

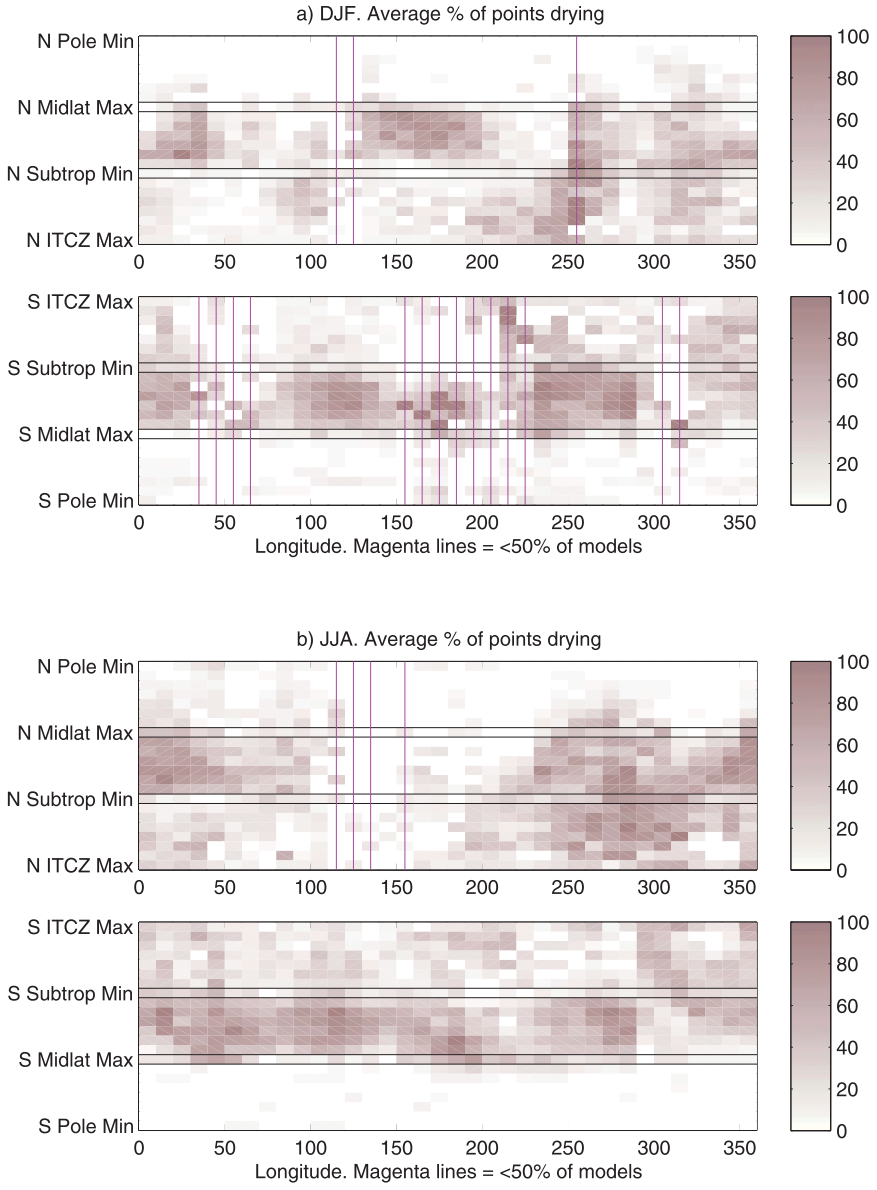

FIG. 11. For each bin of each segment of the (a) December–February and (b) June–August late twentieth-century P climatology profiles in each 10°-longitude zonal mean, the percentage d of latitudes classified in that bin for which seasonal P significantly declines over the twenty-first century (1980–2099), averaged over all GCMs for which the P climatology features are defined at that longitude. Season–hemisphere–longitudes for which less than 50% of the GCMs have these features defined, and thus less than 50% of the GCMs contribute to the plotted profiles, are struck through in magenta as a warning.

increases are surprisingly uncommon in the deep-tropical wet ($P > E$) zones near the ITCZ(s).

Figure 11 shows the *multimodel* average of d as a function of P climate profile segment, bin, and actual longitude strip, for December–February (Fig. 11a) and June–August (Fig. 11b), and Fig. 12 shows the same for w. One can see that the tendency for the models to primarily reduce P poleward (and not equatorward) of the model subtropical P minima is not zonally uniform, at least in these seasons. Instead, in December–February it is very pronounced, even more than Fig. 5a suggests, in the Euro–African (~350°–50°E), northwest Pacific (~120°–200°E), southeast Atlantic (~0°–30°E), south Indian Ocean (~90°–150°E), and southeast Pacific (~230°–290°E) regions (all of which feature active dry-zone–storm-track dynamics), while it is absent or even reversed over much

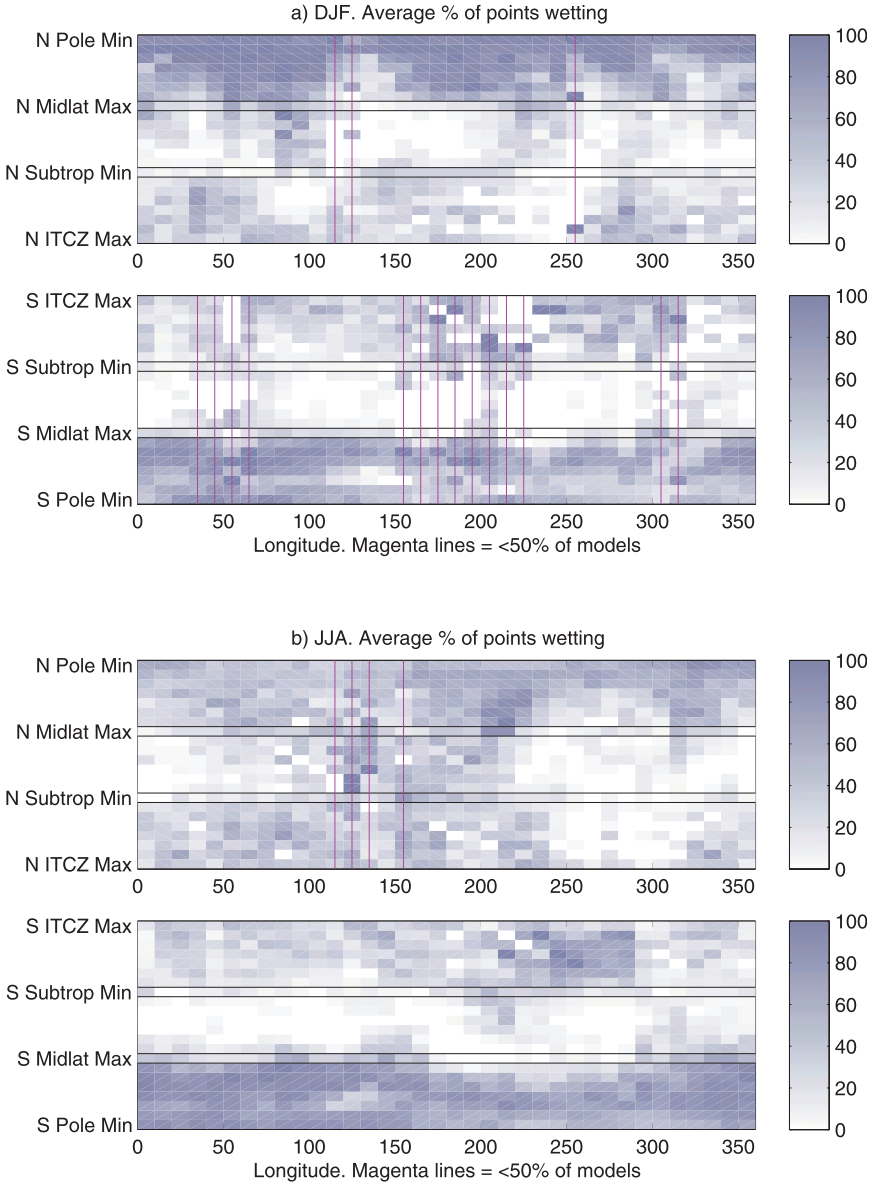

FIG. 12. As in Fig. 11, but for *w*. For each bin of each segment of the (a) December–February and (b) June–August late twentieth-century *P* climatology profiles in each 10°-longitude zonal mean, the percentage *w* of latitudes classified in that bin for which *P* significantly increases over the twenty-first century (1980–2099), averaged over all GCMs for which the *P* climatology features are defined at that longitude. Season–hemisphere–longitudes for which less than 50% of the GCMs have these features defined, and thus less than 50% of the GCMs contribute to the plotted profiles, are struck through in magenta as a warning (identical to those in Fig. 11).

of the American and west Atlantic sectors, especially in the Northern Hemisphere (~230°–340°E). The feature-relative *P* reductions in these latter areas are less robust, but extend much farther equatorward through the heart of the dry zone, than in the former areas. This view usefully complements the analogous message from Fig. 1a, in the traditional ensemble analysis. As discussed more generally in section 4a above, these plots can be interpreted as the *fraction of models that significantly reduce/increase P* in this season in this *P*-feature-relative "location."

The June–August plots (Figs. 11b and 12b) show this zonal asymmetry even more dramatically: the American sector northern subtropics (~240°–320°E), and the south Atlantic subtropics (~330°–10°E) to a lesser extent, frequently feature dominant *P* reductions everywhere from the model ITCZ maxima in *P* nearly to the model

midlatitude maxima in P. In contrast, the aforementioned Euro–African sector, and the entire remainder of the Southern Hemisphere, behave like the means in Fig. 5b, with far more robust drying poleward of the subtropical minima than equatorward; and these responses are again collocated with strong mean-state storm tracks and subtropical highs. (In the remainder of the Northern Hemisphere, robust drying of any sort is less common.)

Also, we can again see that even the local significant ''wet-get-wetter'' P increases at and near the ITCZ maxima in Fig. 12 are consistently less common than these poleward-expansion P decreases (Fig. 11), as we saw in Figs. 5–7 earlier. Similarly, these plots reinforce the earlier impression that at high latitudes poleward of the midlatitude P maxima, drying responses are very rare (Fig. 11), while wetting responses are very common in general and almost universal in local winter (Fig. 12).

In the interest of brevity, we omit the $(P - E)$-climatology-based equivalents of Figs. 11–12; they tell much the same story that the P-based figures did.

5. Summary and discussion

In this study, we asked the following basic question about the well-known robust tendency of general circulation models to reduce precipitation (P) in the subtropics in response to global warming: to what extent does this pattern appear to be a consequence of the well-known poleward shifts of the models' general circulation features, compared to the fixed-circulation, fixed-relative-humidity energetic argument that the subtropical P be reduced? We attempted to address this question by documenting the locations of the significant model seasonal P reductions *relative to the model seasonal climatologies* of P and of $P - E$ (precipitation minus evaporation), and comparing these climate-relative locations to expectations from each of the two mechanisms.

Two very different approaches to this task, a simple multimodel ensemble diagnostic that reproduces IPCC results (section 3) and a novel system for uniformly recording the geography of each individual model's P changes relative to the geography of that model's large-scale hydroclimate features (section 4), have now suggested essentially the same answer to the above question. Namely, the robust model P declines dominate the subtropical flanks of the model midlatitude storm tracks, especially the drier portions, but do not dominate the central nor equatorward parts of the model subtropical dry ($P < E$) zones. This strongly suggests that they mostly consist of known poleward shifts in the model storm tracks (and/or Eulerian subtropical descent regions) and are not *primarily* made up of the ''dry-get-drier'' general moist thermodynamic response to warming. The relative weakness of the robust model P (and $P - E$) increases in the wet tropics, compared to these subtropical/midlatitude declines, further supports this notion that the thermodynamic response of P is not usually locally dominant, at least outside the high latitudes. However, both methods also support localized exceptions to these rules, especially in the subtropical northern Americas and surrounding seas. Both methods also suggest that high-latitude P increases poleward of the initial storm tracks, which could potentially result from either of the two mechanisms, are very robust.

It should be reiterated that $P - E$, unlike P, declines robustly almost throughout the model dry ($P < E$) subtropics. This in fact supports the thermodynamic prediction of an amplifying $P - E$ field, and thus supports the zeroth-order assumptions of constant mass flux and constant relative humidity, which lead to that fundamental prediction. What actually breaks down (cf. Figs. 10 and 8) is the more subtle notion that a robust subtropical $P - E$ response dictates a similarly robust P response.

The P response is a major contributor to model hydrologic change under global warming and is also of fundamental meteorological interest. Another such contributor is evaporation; we also have work in progress analyzing model changes in terrestrial Penman–Monteith potential evapotranspiration under global warming.

Acknowledgments. J. S. would like to thank anonymous reviewer two for very helpful comments; I. Held, Q. Fu, and B. Soden for conceptual conversations; as well as J. M. Wallace for excellent graphical advice. This work was supported by National Science Foundation Grants ATM-0846641 and ATM-0936059, and by a University of Washington Program on Climate Change fellowship to J. S. in 2010.

APPENDIX

Definitions of ITCZ Maxim(a), Subtropical Minima, and Midlatitude Maxima of Meridional Profiles of P and $P - E$

The following definitions seem complicated, but they generally test extremely well against human visual determination across a range of models, seasons, and longitudes, unlike simpler criteria that run into one of the pitfalls detailed below. Furthermore, we can see in section 4b (Figs. 11 and 12) that the interesting model P responses to global warming are generally located outside of the single region (south and east Asia) that

accounts for most of the difficulties encountered by these definitions.

We will first describe this feature definition process for a 10°-zonal-mean pole-to-pole meridional transect $P(y)$ of seasonal P climatology, like that depicted in Fig. 3 (top). To begin, all local maxima (grid latitudes at which $P(y)$ is greater than at either neighboring latitude) along the profile are noted. Of course, many of these are noise or small terrain-induced features and need to be screened out. This is done with a prominence criterion, inspired by, for example, Takahashi (2004): for each local maximum y^* of $P(y)$, we find the first point to the south of y^* with $P > P(y^*)$, take the minimum P value between y^* and this point and subtract this intervening minimum from $P(y^*)$ to obtain the necessary ''descent'' needed to reach the remote ''higher'' point. After performing the same procedure on the north side of y^*, we take the smaller of the southern and northern descents as the *additive prominence* of the maximum at y^*, thus defining prominence as the ''minimum vertical descent needed to reach higher terrain.'' This is well-defined for each local maximum of $P(y)$ except for the absolute, global maximum, to which we assign a prominence of infinity since it has no ''higher terrain'' to reach. Similarly, we define a multiplicative prominence for each y^* using the ratios, rather than the differences, between $P(y^*)$ and P at the intervening minima.

We then set a multiplicative prominence threshold, which will be our main screening tool, at 1.75 (in other words, the additive prominence of the peak above the valley bottom defining it must be at least ¾ the valley bottom elevation, which empirically is almost always true for visually apparent midlatitude and tropical maxima in these profiles). This excludes most of the minor or noise peaks, except for a few in dry regions where P dips close to 0 in the noise minima. These remaining noise peaks are taken care of by setting an additional additive prominence threshold of 0.7 mm day^{-1}.

We can now define the ''tropical maximum'' of the transect, from which all the other feature definitions will ultimately derive, as the highest local maximum of $P(y)$ that lies between latitudes −30° and 30° inclusive and that satisfies the multiplicative prominence threshold.[2] We then recalculate the prominences of all the other maxima, stipulating that this tropical maximum always counts as ''higher ground,'' even if it is in fact lower than the maximum in question (which is possible in longitudes where the ITCZ is relatively weak and there is a strong extratropical storm track). This ensures that minima to one side of the tropical wet belt cannot affect the prominence of maxima on the other side, which would occasionally lead to nonsensical results. We call the peaks that now satisfy both of the prominence thresholds the *nontrivial maxima* of $P(y)$.

Having defined the ''tropical maximum'' in the preceding paragraph, we now proceed to identify any other (i.e., multiple) ITCZ-type peaks of the $P(y)$ transect. The tropical maximum counts as our first ITCZ. Starting from here, we examine the first *non-trivial* maximum to the north. If it lies south of 20° north, *or* is connected to an already-identified ITCZ by a continuous interval of $P(y) > 5$ mm day^{-1}, we include it as an ITCZ, look for the next nontrivial maximum north, and recurse; otherwise, we do not include it as an ITCZ, and we stop. Once we have stopped, we repeat this recursive procedure heading south from the tropical maximum, exchanging the words ''north'' and ''south'' above. This complicated definition of ''ITCZ'' is necessary because local multiple ITCZs are common in these GCM climatologies and because the belts around 20°–32° can host both genuine midlatitude P maxima (e.g., south China in winter or spring, or the midlatitude part of the winter South Pacific convergence zone) and purely ITCZ-type P maxima (e.g., north India in summer). However, the example in Fig. 3 only has a single ITCZ because the multiplicative prominence threshold screens out the peak around 15°S (which is slightly lower than the ITCZ) as trivial.

The *south midlatitude maximum* is then defined to be the most additively prominent nontrivial maximum south of the (south) ITCZ. The *south subtropical minimum* is simply the point with the lowest value of P between the (south) ITCZ and the south midlatitude maximum. If in fact there is no nontrivial maximum south of the ITCZ(s), or if the putative subtropical minimum is poleward of 66.5° south, then these two Southern Hemisphere features are not defined for this particular longitude band. (This is common, for example, in austral summer in the southwest Pacific.) We define (or decline to define) the north midlatitude maximum and north subtropical minimum in exactly the same manner, replacing south with north everywhere above.

Finally, the empirical procedure for the 10°-zonal-mean $(P - E)(y)$ profiles (e.g., top of Fig. 4) is identical, with the following four exceptions. First, since the field is no longer positive definite, we set only a 1 mm day^{-1} additive prominence threshold for a peak to be called nontrivial, with no multiplicative prominence threshold (and thus two ITCZs are defined in the example of Fig. 4). Second, because of this, we define the initial tropical

[2] On the very rare occasion that no such maximum exists, the entire profile is discarded and no P features are detected on the grounds that there is no reasonable way to define a subtropical dry zone if there is no well-defined tropical wet zone.

maximum more carefully: it will be the most prominent nontrivial maximum that is either between −23.5° and 23.5° latitude, or between −30° and 30° latitude and at least 9 mm day^{-1} in value. This seems to be the best resolution for the $P - E$ profiles of the South and East Asian subtropical-zone difficulties described for P above. Third, the $P > 5$ mm day^{-1} "floor" criterion for connecting additional ITCZs is changed to $P - E > 4$ mm day^{-1}. Fourth, we place an additional constraint on *ITCZ-type* peaks only, both the tropical maximum and the subsequently defined maxima: that P must exceed 1.5 mm day^{-1} at land-influenced locations (strip-mean gridcell land fraction > 0.2), or 0.5 mm day^{-1} at ocean-dominated locations (mean land fraction < 0.2), for a local maximum in $P - E$ *whose value is less than +0.05 mm day^{-1}* to be considered nontrivial, even if it has sufficient prominence. This is because meridional changes in E that are solely due to the character of the underlying surface can single-handedly produce pronounced low-latitude peaks in $P - E$ in dry regions. For example, the eastern part of the wintertime Sahara Desert appears as a clear meridional *maximum* in climatological $P - E$ in some models because both P and E in the desert, and thus $P - E$, are basically zero, while both the Mediterranean Sea to the north and the dry-season Sudanian zone to the south have significantly negative $P - E$.

REFERENCES

Allen, M. R., and W. J. Ingram, 2002: Constraints on future changes in the hydrological cycle. *Nature,* **419,** 224–228.

Archer, C. L., and K. Caldeira, 2008: Historical trends in the jet streams. *Geophys. Res. Lett.,* **35,** L08803, doi:10.1029/2008GL033614.

Bengtsson, L., K. I. Hodges, and E. Roeckner, 2006: Storm tracks and climate change. *J. Climate,* **19,** 3518–3543.

Betts, A. K., 1998: Climate–convection feedbacks: Some further issues. *Climatic Change,* **39,** 35–38.

Boer, G. J., 1993: Climate change and the regulation of the surface moisture and energy budgets. *Climate Dyn.,* **8,** 225–239.

Butler, A. H., D. W. J. Thompson, and T. Birner, 2011: Isentropic slopes, down-gradient eddy fluxes, and the extratropical atmospheric circulation response to tropical tropospheric heating. *J. Atmos. Sci.,* **68,** 2292–2305.

Chen, G., J. Lu, and D. M. W. Frierson, 2008: Phase speed spectra and the latitude of surface westerlies: Interannual variability and global warming trend. *J. Climate,* **21,** 5942–5959.

Fischer-Bruns, I., H. von Storch, J. F. Gonzalez-Rouco, and E. Zorita, 2005: Modelling the variability of midlatitude storm activity on decadal to century time scales. *Climate Dyn.,* **25,** 461–476.

Frierson, D. M. W., J. Lu, and G. Chen, 2007: Width of the Hadley cell in simple and comprehensive general circulation models. *Geophys. Res. Lett.,* **34,** L18804, doi:10.1029/2007GL031115.

Fu, Q., and P. Lin, 2011: Poleward shift of subtropical jets inferred from satellite-observed lower-stratospheric temperatures. *J. Climate,* **24,** 5597–5603.

——, C. M. Johanson, J. M. Wallace, and T. Reichler, 2006: Enhanced mid-latitude tropospheric warming in satellite measurements. *Science,* **312,** 1179.

Fyfe, J. C., 2003: Extratropical southern hemisphere cyclones: Harbingers of climate change? *J. Climate,* **16,** 2802–2805.

Held, I., and B. Soden, 2006: Robust responses of the hydrological cycle to global warming. *J. Climate,* **19,** 5686–5699.

Hu, Y., and Q. Fu, 2007: Observed poleward expansion of the Hadley circulation since 1979. *Atmos. Chem. Phys.,* **7,** 5229–5236.

Kidston, J., G. K. Vallis, S. M. Dean, and J. Renwick, 2011: Can the increase in the eddy length scale under global warming cause the poleward shift of the jet streams? *J. Climate,* **24,** 3764–3780.

Lin, J. L., 2007: Interdecadal variability of ENSO in 21 IPCC AR4 coupled GCMs. *Geophys. Res. Lett.,* **34,** L12702, 10.1029/2006GL028937.

Livezey, R. E., and W. Y. Chen, 1983: Statistical field significance and its determination by Monte Carlo techniques. *Mon. Wea. Rev.,* **111,** 46–59.

Lorenz, D. J., and E. T. DeWeaver, 2007: Tropopause height and zonal wind response to global warming in the IPCC scenario integrations. *J. Geophys. Res.,* **112,** D10119, doi:10.1029/2006JD008087.

Lu, J., G. A. Vecchi, and T. J. Reichler, 2007: Expansion of the Hadley cell under global warming. *Geophys. Res. Lett.,* **34,** L06805, doi:10.1029/2006GL028443.

——, G. Chen, and D. M. W. Frierson, 2010: The position of the midlatitude storm track and eddy-driven westerlies in aquaplanet AGCMs. *J. Atmos. Sci.,* **67,** 3984–4000.

Ma, J., S.-P. Xie, and Y. Kosaka, 2012: Mechanisms for tropical tropospheric circulation change in response to global warming. *J. Climate,* **25,** 2979–2994.

Marshall, G. J., 2003: Trends in the southern annular mode from observations and reanalyses. *J. Climate,* **16,** 4134–4143.

McCabe, G. J., M. P. Clark, and M. C. Serreze, 2000: Trends in northern hemisphere surface cyclone frequency and intensity. *J. Climate,* **14,** 2763–2768.

Meehl, G. A., C. Covey, T. Delworth, M. Latif, B. McAvaney, J. F. B. Mitchell, R. J. Stouffer, and K. E. Taylor, 2007a: The WCRP CMIP3 multimodel dataset: A new era in climate change research. *Bull. Amer. Meteor. Soc.,* **88,** 1383–1394.

——, and Coauthors, 2007b: Global climate projections. *Climate Change 2007: The Physical Science Basis,* S. Solomon et al., Eds., Cambridge University Press, 747–845.

Neelin, J. D., M. Munnich, H. Su, J. E. Meyerson, and C. E. Holloway, 2006: Tropical drying trends in global warming models and observations. *Proc. Natl. Acad. Sci. USA,* **103,** 6110–6115.

Previdi, M., and B. G. Liepert, 2007: Annular modes and Hadley cell expansion under global warming. *Geophys. Res. Lett.,* **34,** L22701, doi:10.1029/2007GL031243.

Riviere, G., 2011: A dynamical interpretation of the poleward shift of the jet streams in global warming scenarios. *J. Atmos. Sci.,* **68,** 1253–1272.

Santer, B. D., T. M. L. Wigley, J. S. Boyle, D. J. Gaffen, J. J. Hnilo, D. Nychka, D. E. Parker, and K. E. Taylor, 2000: Statistical significance of trends and trend differences in layer-average atmospheric temperature time series. *J. Geophys. Res.,* **105** (D6), 7337–7356.

Scheff, J., 2011: CMIP3 21st century robust subtropical precipitation declines are mostly mid-latitude shifts. M.S. thesis, Dept. of Atmospheric Sciences, University of Washington,

66 pp. [Available online at http://www.atmos.washington.edu/~jack/Thesis.pdf.]

Seager, R., and Coauthors, 2007: Model projections of an imminent transition to a more arid climate in southwestern North America. *Science,* **316,** 1181–1184.

——, N. Naik, and G. A. Vecchi, 2010: Thermodynamic and dynamic mechanisms for large-scale changes in the hydrological cycle in response to global warming. *J. Climate,* **23,** 4651–4668.

Seidel, D. J., and W. J. Randel, 2007: Recent widening of the tropical belt: Evidence from tropopause observations. *J. Geophys. Res.,* **112,** D20113, doi:10.1029/2007JD008861.

Solomon, S., and Coauthors, 2007: Technical summary. *Climate Change 2007: The Physical Science Basis,* S. Solomon et al., Eds., Cambridge University Press, 19–91.

Takahashi, S., 2004: Algorithms for extracting surface topology from digital elevation models. *Topological Data Structures for Surfaces: An Introduction to Geographical Information Science,* S. Rana, Ed., Wiley, 31–51.

Thompson, D. W. J., J. M. Wallace, and G. C. Hegerl, 2000: Annular modes in the extratropical circulation. Part II: Trends. *J. Climate,* **13,** 1018–1036.

Trenberth, K. E., 1998: Atmospheric moisture residence times and cycling: Implications for rainfall rates with climate change. *Climatic Change,* **39,** 667–694.

Ulbrich, U., J. G. Pinto, H. Kupfer, G. C. Leckebusch, T. Spangehl, and M. Reyers, 2008: Changing northern hemisphere storm tracks in an ensemble of IPCC climate change simulations. *J. Climate,* **21,** 1669–1679.

Wetherald, R. T., and S. Manabe, 2002: Simulation of hydrologic changes associated with global warming. *J. Geophys. Res.,* **107,** 4379, doi:10.1029/2001JD001195.

Wilks, D. S., 2006: *Statistical Methods in the Atmospheric Sciences*. 2nd ed. Academic Press, 627 pp.

Yin, J., 2005: A consistent poleward shift of the storm tracks in simulations of 21st century climate. *Geophys. Res. Lett.,* **32,** L18701, doi:10.1029/2005GL023684.